UDC 519.61:536.4:621.315
Original scientific paper
Received: 03.11.2006.

2D BEM analysis of power cables thermal field

Slavko Vujević and **Petar Sarajčev**
Faculty of Electrical Engineering, Mechanical Engineering and Naval Architecture, University of Split,
Ruđera Boškovića b.b., HR-21000 Split, CROATIA
e-mail: vujevic@fesb.hr

SUMMARY

This paper describes a novel 2D BEM numerical model for analyzing buried power cables thermal field. The total number of power cables and homogeneous subdomains inside the cable trench are completely arbitrary. A novelty in this paper is that a part of unbounded external boundary (earth surface) has been modelled using a new type of boundary elements named infinite boundary elements. Besides, the efficiency of the numerical method developed is based on successful application of analytical integration along linear boundary elements and infinite boundary elements. Using double and multiple global node technique, the correct numerical approximation of the normal flux density at the points with its physical discontinuity has been made possible. Illustrative numerical examples with known analytical solutions are solved.

***Key words**: 2D BEM analysis, infinite boundary element, power cable, thermal field, power cable ampacity.*

1. INTRODUCTION

Computing the maximum current that power cables can sustain from a thermal point of view without the deterioration of any of their mechanical and/or electrical properties is an important design aspect of underground power cables. A typical arrangement of six buried single-core power cables is shown in Figure 1. Power losses refer to the heat generated in cable conducting parts (phase conductors and sheaths) and in cable insulating parts, but the dielectric losses in insulation are neglected. Power losses in phase conductors and sheaths mainly depend on current values. Computing losses in electric power cables [1] is the base for analysis of power cables thermal field. In other words, the heat input rate per unit length of the cable is the significant input datum for analysis of temperature distribution around the underground power cables.

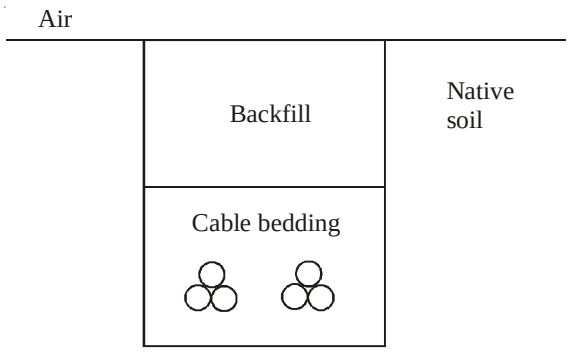

Fig. 1 A typical single-core power cables arrangement

In power cables design, a steady-state thermal analysis has two main variants. The first of them is the temperature rise analysis where desired currents are specified and maximum attained temperatures are computed, and the second variant is the ampacity analysis where desired temperatures are specified and maximum attained currents are computed.

The computation of underground power cables thermal field has been the subject of many papers [2-14]. Significant number of developed numerical models is based on finite difference method [2-6] or finite element method [7-13]. A small number of numerical models is based on boundary element method [14]. In papers [11-13], thermal analysis is based on combination of finite elements and mapped infinite elements. Using mapped infinite elements, an unbounded domain is modelled.

The purpose of this paper is to develop a more accurate 2D BEM model for computing the power cables thermal field. In the considered numerical model, special attention was focused on modelling the infinite boundaries.

2. NUMERICAL MODEL

2.1 Description of illustrative example

2D boundary element method is used to compute the cables surface temperature based on the heat input rate. The application of the method is illustrated for buried singlecore cable case (Figure 2). In this example, the heterogeneous domain Ω is subdivided into two homogeneous and isotropic subdomains. Singlecore cable is located in the rectangular trench (subdomain Ω_1), and subdomain Ω_2 is unbounded native soil. It is convenient to assume that the temperature on the earth surface is constant and equal to the ambient temperature (T_{amb}). In other words, the temperature on the earth surface is equal to the temperature at infinity.

The Dirichlet boundary condition:

$$T = T_{amb} \tag{1}$$

is homogenized in such a way that a new temperature function is defined:

$$\bar{T} = T - T_{amb} \tag{2}$$

For new temperature function $\bar{T}$, the Dirichlet boundary condition on the earth surface and at infinity is equal to zero ($\bar{T} = 0$). Firstly, the temperature $\bar{T}$ is computed and then by using Eq. (2) temperature T is obtained.

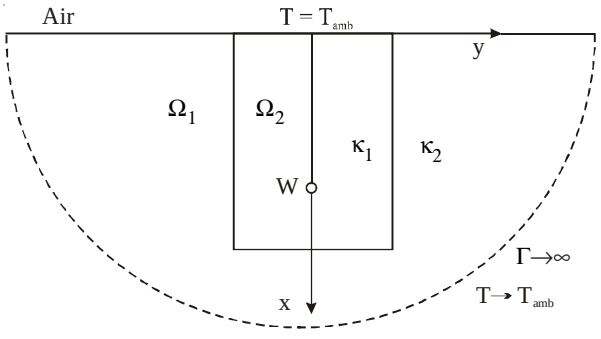

Fig. 2 Geometry of the illustrative single-core power cable case

2.2 Application of the BEM to 2D temperature Poisson problem

The temperature distribution inside of the subdomain Ω_p is described by Poisson differential equation:

$$\Delta\bar{T} = -\sum_{s=1}^{NSC} \delta_{ps} \cdot \frac{W_s}{\kappa_p} \cdot \delta(\vec{r} - \vec{r}_s) \tag{3}$$

where:

κ_p - thermal conductivity of the medium p,
W_s - the total heat input rate of the s^{th} cable (source),
$\vec{r}$ - the position vector of the field point,
$\vec{r}_s$ - the position vector of the source point,
$\delta(\vec{r} - \vec{r}_s)$ - the Dirac delta function,
NSC - the total number of sources,

$$\delta_{ps} = \begin{cases} 1, & \text{if } s\text{-th source} \in \Omega_p \\ 0, & \text{if } s\text{-th source} \notin \Omega_p \end{cases}$$

For the discretization of the external and internal boundaries, linear boundary elements with two local nodes were used (Figure 3). Due to simplicity, in Figure 3, the boundaries discretization is realized with a small total number of boundary elements.

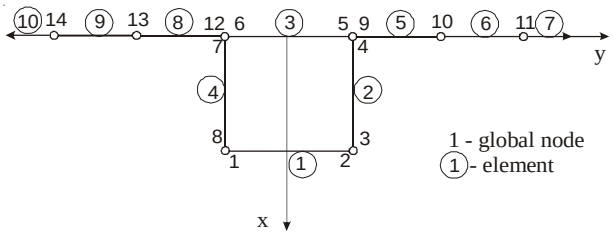

Fig. 3 Discretization of the external and internal boundaries

In intersection points of boundary elements, in which there is a continuity of the normal flux density, only one global node is located. However, at the boundary elements intersection point in which there is a discontinuity of the normal flux density, the double node technique must be used, i.e. two global nodes are located at such a point.

At the intersection points of several boundary elements, the correct approximation of the normal flux density imposes the use of the multiple node technique, i.e. at the intersection point of n boundary elements, n global nodes are located.

The unbounded external boundary has been modelled using a new type of boundary element with only one local node (elements 7 and 10 in Figure 3), which can be named infinite boundary element.

The temperature $\bar{T}_k$ at the point $P_k(x_k,y_k)$, which is located within subdomain Ω_p or on its boundary, is described by the following expression:

$$C_k \cdot \bar{T}_k = \sum_{r=1}^{NSD} a_{pr} \cdot \int_{\Gamma_{pr} \setminus P_k} \left(\frac{\psi_k \cdot q}{\kappa_p} - \bar{T} \cdot \frac{\partial \psi_k}{\partial n} \right) \cdot d\Gamma + \sum_{s=1}^{NSC} \frac{W_s}{\kappa_p} \cdot \psi_{ks} \cdot \delta_{ps} \tag{4}$$

where C_k is the constant [15], which depends on the position of the point P_k, NSD is the total number of subdomains,

$$a_{pr} = \begin{cases} 1 & if \quad p \le r \\ 0 & if\ there\ is\ no\ interface\ \Gamma_{pr} \\ -1 & if \quad p > r \end{cases}$$

is the constant depending on the normal $\vec{n}_{pr}$ direction,

$$q = \begin{cases} \kappa_p \cdot \dfrac{\partial \bar{T}}{\partial n}, \ p \le r, \\ \\ \kappa_r \cdot \dfrac{\partial \bar{T}}{\partial n}, \ p > r, \end{cases}$$

is the flux density along normal vector $\vec{n}_{pr}$, while κ_p and κ_r are material conductivities. In developed numerical model it has been assumed that the unitary normal vector $\vec{n}_{pr}$ to the interface between two subdomains has its direction from subdomain p to subdomain r, where $p \le r$.

The weighted function:

$$\Psi_k = \frac{1}{2 \cdot \pi} \cdot ln \frac{1}{\sqrt{(x - x_k)^2 + (y - y_k)^2}} + A \tag{5}$$

is a fundamental solution of the Poisson equation, Eq. (3), where:

$$A = \frac{1}{2 \cdot \pi} \cdot ln(100 \cdot d_{max}) \tag{6}$$

is the constant which has been introduced to improve numerical stability of the algorithm, and d_{max} is the maximum distance between the nodes of the boundary element grid.

According to Eqs. (5) and (6), the weighted function ψ_{ks}, introduced by Eq. (4), is described by the following equation:

$$\psi_{ks} = \frac{1}{2\pi} \cdot ln \frac{100 \cdot d_{max}}{\left| \sqrt{(x_k - x_s)^2 + (y_k - y_s)^2} \right|} \tag{7}$$

2.3 Local co-ordinate system of the boundary element

In this paper, the usual numerical integration along the single boundary element is totally substituted by analytical integration. That was the reason to introduce a boundary element local co-ordinate system (u,v) according to Figure 4. Local co-ordinates (u,v) of the point P are computed from its global co-ordinates (x,y) according to the following equations:

$$u = \frac{2}{\ell} \cdot \left[(x - x_M) \cdot (x_2 - x_M) + (y - y_M) \cdot (y_2 - y_M) \right] \tag{8}$$

$$v = \sqrt{(x - x_M)^2 + (y - y_M)^2 - u^2} \tag{9}$$

$$x_M = \frac{x_1 + x_2}{2} \quad ; \quad y_M = \frac{y_1 + y_2}{2} \tag{10}$$

where ℓ is the boundary element length; (x_1, y_1) are global co-ordinates of the local node *1* and (x_2, y_2) are global co-ordinates of the local node 2.

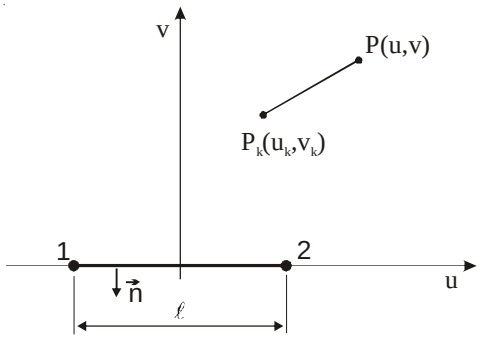

Fig. 4 Linear boundary element in the local co-ordinate system

For linear boundary elements, the temperature distribution $\bar{T}$ and the normal flux density q along the j^{th} boundary element are approximated by:

$$\bar{T} = \sum_{i=1}^{2} N_{ji} \cdot \bar{T}_{ji} \tag{11}$$

$$Q = \sum_{i=1}^{2} N_{ji} \cdot Q_{ji} \tag{12}$$

where N_{ji} is the shape function joined to the i^{th} local node of the j^{th} boundary element, $\bar{T}_{ji}$ is the temperature at the i^{th} local node of the j^{th} boundary element, and Q_{ji} is the value of the normal component of the flux density at the i^{th} node of the j^{th} boundary element.

The shape functions are defined in the local co-ordinate system (u,v) as it follows:

$$N_{j1} = \frac{\ell - 2u}{2 \cdot \ell} \tag{13}$$

$$N_{j2} = \frac{\ell + 2u}{2 \cdot \ell} \tag{14}$$

For simplicity, the local nodes of each boundary element are positioned so that the normal always has the position as shown in Figure 4.

2.4 Infinite boundary element

Because the earth surface is unbounded, the part of the boundary between the air and the earth has been modelled using two infinite boundary elements (Figure 5).

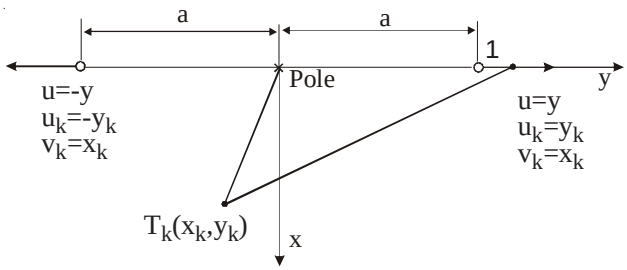

Fig. 5 Infinite boundary elements

Along the infinite boundary elements, the temperature is equal to zero ($\overline{T} = 0$). Therefore, only normal component of the flux density q along infinite boundary element has to be approximated. The poles of infinite boundary elements have to be located in the center of cable trench external boundary. Because (in this paper) the origin of global coordinate system (x,y) is located in the center of cable trench external boundary, the poles of the infinite boundary elements are located in the origin of the global co-ordinate system (Figure 5). The intensity of normal component of the flux density decreases with the square of the distance between field point and infinity boundary element pole and the normal component of the flux density has been approximated by the following equation:

$$Q = \frac{a^2}{u^2} \cdot Q_{j1} = \frac{a^2}{y^2} \cdot Q_{j1} = N_{j1} \cdot Q_{j1} \qquad (15)$$

where N_{j1} is the shape function joined to the local node of the j^{th} (infinite) boundary element, and Q_{j1} is the value of the normal component of the flux density at the node of the j^{th} boundary element. For the difference of linear boundary element, which has two local nodes, the infinite boundary element has only one global node.

2.5 System of linear equations

The integration along the boundary curve $\Gamma_{pr} \setminus P_k$ is equal to the sum of the integrals along linear boundary elements and infinite boundary elements, then, according to Eqs. (4), (11), (12) and (15), the temperature $\overline{T}_k$ at the point P_k belonging to the p^{th} subdomain is described by:

$$C_k \cdot \overline{T}_k = \sum_{r=1}^{NSD} a_{pr} \cdot \left\{ \sum_{j=1}^{NE} \left[\sum_{i=1}^{NLNJ} \left(\frac{1}{\kappa_p} \int_{\Gamma_{prj} \setminus P_k} \psi_k \cdot N_{ji} \cdot d\Gamma \right) \cdot Q_{ji} - \sum_{i=1}^{NLNJ} \left(\int_{\Gamma_{prj} \setminus P_k} N_{ji} \cdot \frac{\partial \psi_k}{\partial n} \cdot d\Gamma \right) \cdot \overline{T}_{ji} \right] \right\} + \sum_{s=1}^{NSC} \frac{W_s}{\kappa_p} \cdot \psi_{ks} \cdot \delta_{ps} \qquad (16)$$

where NE is the total number of elements (boundary elements + infinite boundary elements) in the whole domain Ω, $NLNJ$ is the total number of local nodes of j^{th} element, and Γ_{prj} is a part of the boundary Γ_{pr} belonging to the j^{th} element.

The expression (16) can be written as:

$$C_k \cdot \overline{T}_k = \sum_{r=1}^{NSD} \sum_{j=1}^{NE} \sum_{i=1}^{NLNJ} \left(G^*_{kji} \cdot Q_{ji} - H^*_{kji} \cdot \overline{T}_{ji} \right) + \sum_{s=1}^{NSC} \frac{W_s}{\kappa_p} \cdot \psi_{ks} \cdot \delta_{ps} \qquad (17)$$

where:

$$G^*_{kji} = a_{pr} \cdot \frac{1}{\kappa_p} \cdot \int_{\Gamma_{prj} \setminus P_k} \psi_k \cdot N_i \cdot d\Gamma \qquad (18)$$

$$H^*_{kji} = a_{pr} \cdot \int_{\Gamma_{prj} \setminus P_k} N_i \cdot \frac{\partial \psi_k}{\partial n} \cdot d\Gamma \qquad (19)$$

In a case of infinite boundary element, Eq. (18) can be written as:

$$G^*_{kj1} = a_{pr} \cdot \frac{1}{\kappa_p} \cdot \int_a^\infty N_{j1} \cdot \psi_k \cdot du = a_{pr} \cdot \frac{a^2}{\kappa_p} \cdot \int_a^\infty \frac{1}{u^2} \cdot \psi_k \cdot du \qquad (20)$$

and H^*_{kj1} is not computed because $\bar{T}=0$ along the infinite boundary element.

The coefficients G^*_{kji} and H^*_{kji} are computed by analytical integration [16].

Using global nodes notation, the system of Eqs. (17) can be written:

$$C_k \cdot \bar{T}_k = \sum_{m=1}^{NN} \left(G_{km} \cdot Q_m - H_{km} \cdot \bar{T}_m \right) + \sum_{s=1}^{NSC} \frac{W_s}{\kappa_p} \cdot \psi_{ks} \cdot \delta_{ps} \tag{21}$$

where *NN* is the total number of global nodes, $\bar{T}_m$ is the temperature at the m^{th} global node and Q_m is the normal component of the flux density at the m^{th} global node.

The unknown temperatures and normal densities at the global nodes could be computed using the point collocation method. It is useful to assume that the total number of collocation points is equal to the total number of unknowns. In other words, one collocation point per subdomain is joined to each global node with at least one unknown.

If at a single point there is only one global node (single global node case), then the joined collocation point is located at the observed node. However, if at a single point there are two global nodes (double global node case) or several global nodes (multiple global node case), then the joined collocation points are moved from the observed nodes along the associated boundary elements by one-quarter of the boundary element length. The system of linear equations obtained by this algorithm is regular in all cases.

Collocation point method, applied to Eq. (21), gives the next system of linear equations:

$$\begin{aligned} & C_k \cdot \left(\alpha \cdot \bar{T}_k + \beta \cdot \bar{T}_d \right) = \\ & = \sum_{m=1}^{NN} \left(G_{km} \cdot Q_m - H_{km} \cdot \bar{T}_m \right) + \sum_{s=1}^{NSC} \frac{W_s}{\kappa_p} \cdot \psi_{ks} \cdot \delta_{ps}, \\ & k = 1, 2, ..., NU \end{aligned} \tag{22}$$

where *NU* is the total number of unknowns, $\bar{T}_k$ is k^{th} global node temperature, $\bar{T}_d$ is d^{th} global node temperature, while the values of the α_k and β_k are $\alpha_k=1$ and $\beta_k=0$ if the collocation point is located in the k^{th} global node, and $\alpha_k=0.75$ and $\beta_k=0.25$ if the collocation point P_k is moved from the k^{th} node.

The system of linear Eqs. (22) in matrix notation can be written as:

$$[G] \cdot \{Q\} - [H] \cdot \{\bar{T}\} + \{\bar{T}_s\} = [C] \cdot \{\bar{T}\} \tag{23}$$

The system of linear Eqs. (23) is regular. However, in points with more than one global node, the temperature continuity, which must be satisfied, can be significantly interrupted. Therefore, due to numerical stability, a new equations have been added to this system. These additional equations equalize the temperatures of the global nodes located in the same point.

The extended system of linear algebraic equations can be written in the following form:

$$[A] \cdot \{X\} = \{B\} \tag{24}$$

where $\{X\}$ is the vector of unknowns.

By solving the system of linear Eqs. (24), the unknown normal flux densities and temperatures at all global nodes can be computed. In general case, this is a situation when we wish to find the least squares solution to an over-determined set of linear equations. Since this set of equations is very close to singular, the system of Eqs. (24) has been solved using the algorithm based on singular value decomposition [17].

3. ANALYTICAL SOLUTION FOR ILLUSTRATIVE EXAMPLE

For chosen illustrative example, presented in Figure 2, an analytical solution for temperature $\bar{T}$ inside of cable trench (subdomain Ω_1) can be obtained using the method of images. In the first step, the Dirichlet boundary condition $\bar{T}=0$ on the earth surface is satisfied using the method of images. The source and both subdomains are reflected in relation to the earth surfaces (Figure 6). In the second step, the original source and its image in relation to the earth surface (Figure 6) is reflected infinite number of times in relation to modified subdomain Ω_1 boundaries [18].

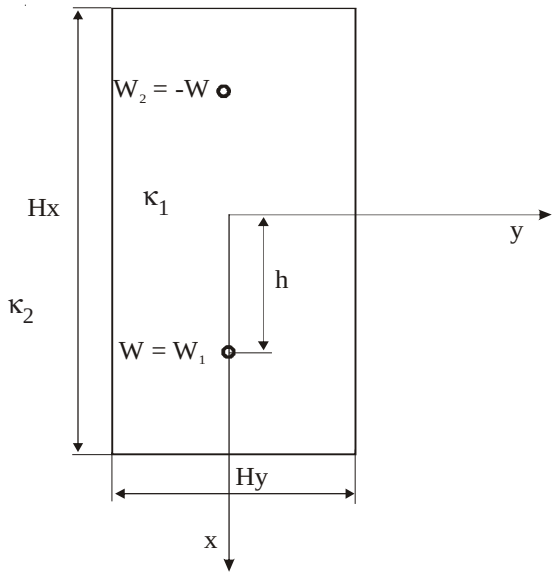

Fig. 6 Problem geometry modified by method of images

Finally, the next analytical expression for temperature distribution inside original subdomain Ω_1 (Figure 2) has been obtained:

$$\bar{T} = \bar{T}(x,y) = \frac{W}{2\pi\cdot\kappa_1}\cdot ln\frac{\sqrt{(x+x_{11})^2+(y-y_{11})^2}}{\sqrt{(x-x_{11})^2+(y-y_{11})^2}} +$$

$$+\frac{W}{2\pi\cdot\kappa_1}\cdot\sum_{k=2}^{\infty}R^{k-1}\left[ln\frac{\sqrt{(x+x_{11})^2+(y-y_{1k})^2}}{\sqrt{(x-x_{11})^2+(y-y_{1k})^2}}+ln\frac{\sqrt{(x+x_{11})^2+(y-y_{2k})^2}}{\sqrt{(x-x_{11})^2+(y-y_{2k})^2}}\right]+$$

$$+\frac{W}{2\pi\cdot\kappa_1}\cdot\sum_{j=2}^{\infty}R^{j-1}\left[ln\frac{\sqrt{(x+x_{1j})^2+(y-y_{11})^2}}{\sqrt{(x-x_{1j})^2+(y-y_{11})^2}}+ln\frac{\sqrt{(x+x_{2j})^2+(y-y_{11})^2}}{\sqrt{(x-x_{2j})^2+(y-y_{11})^2}}\right]+ \qquad (25)$$

$$+\frac{W}{2\pi\cdot\kappa_1}\cdot\sum_{j=2}^{\infty}\sum_{k=2}^{\infty}\frac{1}{2}R^{j+k-3}\cdot(R-1)\cdot\left[ln\frac{\sqrt{(x+x_{1j})^2+(y-y_{1k})^2}}{\sqrt{(x-x_{1j})^2+(y-y_{1k})^2}}+ln\frac{\sqrt{(x+x_{2j})^2+(y-y_{1k})^2}}{\sqrt{(x-x_{2j})^2+(y-y_{1k})^2}}\right]+$$

$$+\frac{W}{2\pi\cdot\kappa_1}\cdot\sum_{j=2}^{\infty}\sum_{k=2}^{\infty}\frac{1}{2}R^{j+k-3}\cdot(R-1)\cdot\left[ln\frac{\sqrt{(x+x_{1j})^2+(y-y_{2k})^2}}{\sqrt{(x-x_{1j})^2+(y-y_{2k})^2}}+ln\frac{\sqrt{(x+x_{2j})^2+(y-y_{2k})^2}}{\sqrt{(x-x_{2j})^2+(y-y_{2k})^2}}\right]$$

where:

$$R=\frac{\kappa_1-\kappa_2}{\kappa_1+\kappa_2} \qquad (26)$$

is the geometric reflection factor,

$$x_{11}=h \;\;;\;\; x_{12}=H_x-h;\;\; x_{22}=-H_x-h$$
$$x_{1j}=-x_{2,j-1}+H_x \;\;;\;\; j=3,4,5,... \qquad (27)$$
$$x_{2j}=-x_{1,j-1}-H_x \;\;;\;\; j=3,4,5,...$$

and:

$$y_{11}=0 \;\;;\;\; y_{21}=H_y \;\;;\;\; y_{22}=-H_y$$
$$y_{1k}=y_{1,k-1}+H_y \;\;;\;\; k=2,3,4,... \qquad (28)$$
$$y_{2k}=-y_{1k} \;\;;\;\; k=2,3,4,...$$

Distances H_x, H_y and h are defined in Figure 6.

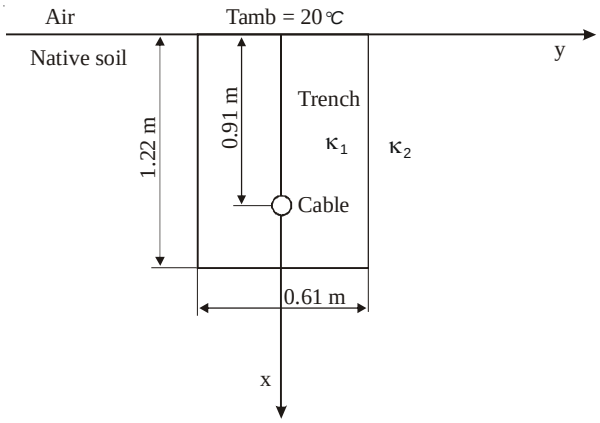

Fig. 7 Single-core cable in a trench

4. NUMERICAL EXAMPLES

On the basis of the presented theory a software package EarthCable has been developed for the numerical analysis of buried power cables thermal field. For the illustration, numerical examples with known analytical solutions are presented. In all examples the geometry is identical; the single-core cable is placed in a *0.61x1.22 m* trench (Figure 7). Internal boundary is divided into 50 linear boundary elements, and external boundary is divided into 30 linear boundary elements and two infinite boundary elements. The distance between poles and nodes of infinite boundary elements is: *a=15 m*; external radius of single-core cable is: *r=0.0255 m*.

In all numerical examples, the temperature $T_0=90°C$ at the cable surface is input datum, and output datum is the heat input rate per unit length of the cable *W*. Comparison of the heat input rates *W* computed by EarthCable with the exact values is presented in Table 1 for $\kappa_1 \geq \kappa_2$ and in Table 2 for $\kappa_2 \geq \kappa_1$.

According to Tables 1 and 2, the numerical procedure based on 2D BEM is very accurate. For the same input data, the values computed by numerical model based on BEM without infinite boundary elements [14] and by numerical model based on FEM [10] are presented in Table 3. According to Table 1 and Table 3, the numerical model developed in this paper is much more accurate than both other numerical models.

Table 1 Comparison of the computed heat input rates for $\kappa_1 \geq \kappa_2$

$\frac{\kappa_1}{\kappa_2}$	κ_1 [W/°Cm]	κ_2 [W/°Cm]	Exact W [W/m]	Computed W [W/m]	Error [%]
1	0.67	0.67	69.045	69.059	0.020
1.49	1.0	0.67	90.815	90.867	0.057
1.66	1.11	0.67	97.423	97.471	0.049
1.87	1.25	0.67	105.505	105.537	0.030
2.13	1.43	0.67	115.471	115.466	-0.004
2.49	1.67	0.67	128.196	128.113	-0.065
2.99	2.0	0.67	144.925	144.703	-0.153
3.73	2.5	0.67	169.136	168.665	-0.278
4.97	3.33	0.67	207.479	206.592	-0.428
5.97	4.0	0.67	237.404	236.235	-0.492
10	6.7	0.67	353.393	351.841	-0.439

Table 2 Comparison of the computed heat input rates for $\kappa_2 \geq \kappa_1$

$\frac{\kappa_2}{\kappa_1}$	κ_1 [W/°Cm]	κ_2 [W/°Cm]	Exact W [W/m]	Computed W [W/m]	Error [%]
1	0.67	0.67	69.045	69.059	0.020
1.49	0.67	1.0	77.343	77.285	-0.075
3.73	0.67	2.5	93.489	93.298	-0.204
4.97	0.67	3.33	97.243	97.047	-0.202
10	0.67	6.7	103.803	103.648	-0.149
50	0.67	33.5	109.908	109.860	-0.044
100	0.67	67.0	110.740	110.711	-0.026

Table 3 Comparison of heat input rates computed by BEM [14] and FEM [10] with exact values

κ_1 [W/°Cm]	κ_2 [W/°Cm]	Exact W [W/m]	BEM [14]		FEM [10]	
			W [W/m]	Error [%]	W [W/m]	Error [%]
1.0	0.67	90.815	91.5	0.754	98.16	8.087
1.11	0.67	97.423	98.79	1.403	105.25	8.034
1.25	0.67	105.505	107.74	2.118	113.64	7.711
1.43	0.67	115.471	119.02	3.073	124.0	7.386
1.67	0.67	128.196	133.78	4.356	137.18	7.008
2.0	0.67	144.925	154.03	6.283	154.69	6.737
2.5	0.67	169.136	183.73	8.628	179.61	6.192
3.33	0.67	207.479	234.15	12.855	219.15	5.625

5. CONCLUSIONS

The numerical model for 2D BEM analysis of buried power cables thermal field has been developed. External and internal boundaries are divided into linear boundary elements and a part of unbounded external boundary (earth surface) has been modelled using a new type of boundary elements named infinite boundary elements. All coefficients for the obtained system of linear equations are computed using the analytical integration along linear boundary elements and infinite boundary elements. The software package developed upon presented theory, gives highly accurate results in a short execution time. Other advantages of the developed numerical model are the simplicity of use and low input data requirements. Presented simple numerical examples have confirmed the correctness of the presented theory and the high accuracy of the developed software package.

6. REFERENCES

[1] I. Sarajčev, M. Majstrović and I. Medić, Calculation of losses in electric power cables as the base of cable temperature analysis, Proc. of the 6th Int. Conf. on Advanced Computational Methods in Heat Transfer, Eds. B. Sunder and C.A. Brebbia, WIT Press, Southampton, pp. 529-537, 2000.

[2] M.A. Hanna, A.Y. Chikhani and M.M.A. Salama, Thermal analysis of power cables in multilayered soil - Part 1: Theoretical model, *IEEE Transactions on Power Delivery*, Vol. 8, No. 3, pp. 761-771, 1993.

[3] M.A. Hanna, A.Y. Chikhani and M.M.A. Salama, Thermal analysis of power cables in multilayered soil - Part 2: Practical considerations, *IEEE Transactions on Power Delivery*, Vol. 8, No. 3, pp. 772-778, 1993.

[4] M.A. Hanna, A.Y. Chikhani and M.M.A. Salama, Thermal analysis of power cables in multilayered soil - Part 3: Case of two cables in a trench, *IEEE Transactions on Power Delivery*, Vol. 9, No. 1, pp. 572-578, 1994.

[5] M.A. Hanna, A.Y. Chikhani and M.M.A Salama, Thermal analysis of power cables systems in a trench in multilayered soil, *IEEE Transactions on Power Delivery*, Vol. 13, No. 2, pp. 304-309, 1998.

[6] T.A. Haskew, R.F. Carwile and L.L.Grigsby, An algorithm for steady-state thermal analysis of electrical cables with radiation by reduced Newton-Raphson techniques, *IEEE Transactions on Power Delivery*, Vol. 9, No. 1, pp. 526-533, 1994.

[7] E. Tarasiewicz, E. Kuffel and S. Grzybowski, Calculation of temperature distributions within cable trench backfill and the surrounding soil, *IEEE Transactions on Power Apparatus and Systems*, Vol. 104, No. 8, pp. 1973-1978, 1985.

[8] M.A. El-Kady, Calculation of the sensitivity of power cable ampacity to variations of design and environmental parameters, *IEEE Transactions on Power Apparatus and Systems*, Vol. 103, No. 8, pp. 2043-2050, 1984.

[9] M.A. Kellow, A numerical procedure for the calculation of the temperature rise and ampacity of underground cables, *IEEE Transactions on Power Apparatus and Systems*, Vol. 100, No. 7, pp. 3322-3330, 1981.

[10] J.K. Mitchell and O.N. Abdel-Hadi, Temperature distributions around buried cables, *IEEE Transactions on Power Apparatus and Systems*, Vol. 98, No. 4, pp. 1158-1166, 1979.
[11] F. Damjanić and D.R.J. Owen, Mapped infinite elements in transient thermal analysis, *Computer and Structures*, Vol. 19, No. 4, pp. 673-687, 1984.
[12] N. Kovač, I. Sarajčev and D. Poljak, Nonlinearcoupled electricthermal modeling of underground cable systems, *IEEE Transactions on Power Delivery*, Vol. 21, No. 1, pp. 4-14, 2006.
[13] N. Kovač, I. Sarajčev and D. Poljak, A numerical-stochastic technique for underground cable systems design, *IEE Proceedings Generation, Transmission and Distribution*, Vol. 153, No. 2, pp. 181-186, 2006.
[14] G. Gela and J.J. Dai, Calculation of thermal fields of underground cables using the boundary element method, *IEEE Transactions on Power Delivery*, Vol. 3, No. 4, pp. 1341-1347, 1988.
[15] C.A. Brebbia and S. Walker, *Boundary Element Techniques in Engineering*, Newnes-Butterworths, London, 1980.
[16] S. Vujević, V. Srzentić-Gazzari and S. Gazzari, Two-dimensional BEM for analysis of potential Laplace problems, *International Journal for Engineering Modelling*, Vol. 15, No. 1-4, pp. 45-50, 2002.
[17] W.H. Press, S.A. Teukolsky, W.T Vetterling and B.P Flanerry, *Numerical Recipes in FORTRAN – The Art of Scientific Computing*, Second edition, Cambridge University Press, New York, 1992.
[18] J.V. Schmill, Mathematical solution to the problem of the control of the thermal environment of buried cables, *AIEE Transactions, Part III*, Vol. 79, No. 1, pp. 175-185, 1960.

2D BEM PRORAČUN TEMPERATURNOG POLJA ELEKTROENERGETSKIH KABELA

SAŽETAK

U ovom je radu opisan novi 2D BEM numerički model za proračun temperaturnog polja ukopanih elektroenergetskih kabela. Ukupan broj kabela i ukupan broj homogenih podpodručja unutar kabelskog kanala potpuno su proizvoljni. Novina u ovom radu je to što je dio otvorene vanjske granice (površina tla) modeliran pomoću novog tipa graničnog elementa nazvanog beskonačni granični element. Osim toga, djelotvornost numeričkog postupka zasnovana je na uspješnoj primjeni analitičke integracije duž linearnih graničnih elemenata te duž beskonačnih graničnih elemenata. Upotrebom tehnike dvostrukih i višestrukih globalnih čvorova, dobiveno je fizikalno ispravno rješenje za normalnu komponentu gustoće toka i u točkama u kojima postoji njezin diskontinuitet. Riješeni su pokazni primjeri koji imaju poznato analitičko rješenje.

***Ključne riječi**: 2D BEM proračun, beskonačni granični element, elektroenergetski kabel, temperaturno polje, dozvoljena strujna opteretivost kabela.*